Journal of Medicinal Chemistry

ARTICLE

pubs.acs.org/jmc

Potent, Metabolically Stable Benzopyrimido-pyrrolo-oxazine-dione (BPO) CFTR Inhibitors for Polycystic Kidney Disease

David S. Snyder,[†,‡] Lukmanee Tradtrantip,[†] Chenjuan Yao,[†] Mark J. Kurth,[‡] and A. S. Verkman*[,†]

[†]Departments of Medicine and Physiology, University of California, San Francisco, California 94143-0521, United States

[‡]Department of Chemistry, University of California, Davis, California 95616, United States

Supporting Information

ABSTRACT: We previously reported the discovery of pyrimido-pyrrolo-quinoxalinedione (PPQ) inhibitors of the cystic fibrosis transmembrane conductance regulator (CFTR) chloride channel and showed their efficacy in an organ culture model of polycystic kidney disease (PKD) (J. Med. Chem. 2009, 52, 6447−6455). Here, we report related benzopyrimido-pyrrolo-oxazinedione (BPO) CFTR inhibitors. To establish structure−activity relationships and select lead compound(s) with improved potency, metabolic stability, and aqueous solubility compared to the most potent prior compound **8** (PPQ-102, $IC_{50} \sim 90$ nM), we synthesized 16 PPQ analogues and 11 BPO analogues. The analogues were efficiently synthesized in 5−6 steps and 11−61% overall yield. Modification of **8** by bromine substitution at the 5-position of the furan ring, replacement of the secondary amine with an ether bridge, and carboxylation, gave 6-(5-bromofuran-2-yl)-7,9-dimethyl-8,10-dioxo-11-phenyl-7,8,9,10-tetrahydro-6*H*-benzo[*b*]pyrimido [4′,5′:3,4]pyrrolo [1,2-*d*][1,4]oxazine-2-carboxylic acid **42** (BPO-27), which fully inhibited CFTR with $IC_{50} \sim 8$ nM and, compared to **8**, had >10-fold greater metabolic stability and much greater polarity/aqueous solubility. In an embryonic kidney culture model of PKD, **42** prevented cyst growth with $IC_{50} \sim 100$ nM. Benzopyrimido-pyrrolo-oxazinediones such as **42** are potential development candidates for antisecretory therapy of PKD.

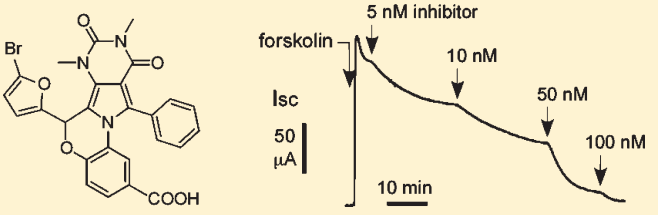

INTRODUCTION

Polycystic kidney disease (PKD) is one of the most common human genetic diseases and a major cause of chronic renal insufficiency requiring dialysis and kidney transplantation.[1] Cyst growth in autosomal dominant polycystic kidney disease (ADPKD) involves progressive fluid accumulation.[2,3] Fluid secretion into the cyst lumen requires chloride secretion by the cystic fibrosis transmembrane conductance regulator (CFTR) protein,[4,5] a cAMP-regulated chloride channel in which loss-of-function mutations cause the genetic disease cystic fibrosis.[6] CFTR is expressed strongly in epithelial cells lining cysts in ADPKD.[7] Cystic fibrosis (CFTR-deficient) mice are resistant to cyst formation, and CFTR inhibitors block cyst formation in cell/organ culture and in vivo models.[8,9] In rare families affected with ADPKD and cystic fibrosis, individuals with both ADPKD and CF have less severe renal disease than those with ADPKD only.[10−12] Cyst expansion in ADPKD also requires cyst epithelial cell proliferation involving mTor signaling,[13,14] which is the basis of several "anti-proliferative" therapies under development.[15−18] "Antisecretory" (CFTR inhibition) therapy is predicted to complement antiproliferative therapy or be effective alone in life-long treatment of ADPKD.

We identified several classes of small-molecule CFTR inhibitors by high-throughput screening (reviewed in ref 19). Thiazolidinone-class CFTR inhibitors such as $CFTR_{inh}$-172 (Figure 1) act on the cytoplasmic side of the plasma membrane at a site near the CFTR pore to block CFTR chloride conductance.[20−22] $CFTR_{inh}$-172 has been used widely as a research tool to study CFTR function in cell culture, ex vivo tissues, and animal models. $CFTR_{inh}$-172 inhibits CFTR, with IC_{50} in the range of 300−3000 nM, depending on cell type and membrane potential, and was shown to have low toxicity and metabolic stability with primarily renal excretion.[21,23] The tetrazolo-substituted thiazolidinone Tetrazolo-172 (Figure 1) has improved water solubility compared to $CFTR_{inh}$-172,[24] reducing cyst expansion in organ culture and mouse models of PKD.[25] A second class of small-molecule CFTR inhibitors, the glycine hydrazides, such as GlyH-101 (Figure 1), block CFTR at an external site within the CFTR pore.[26] Membrane-impermeant, nonabsorbable conjugates of glycine hydrazides with polyethylene glycols (Figure 1)[27,28] and lectins[29] inhibit CFTR with IC_{50} down to 50−100 nM when added at the mucosal cell surface and were effective in rodent models of secretory diarrheas such as cholera. An absorbable glycine hydrazide, phenyl-GlyH-101 (Figure 1), reduced cyst growth in PKD.[25]

Additional small molecule screening yielded pyrimido-pyrrolo-quinoxalinedione (PPQ) compounds, which were the first uncharged, and thus membrane-potential insensitive, CFTR inhibitors.[30] 7,9-Dimethyl-11-phenyl-6-(5-methylfuran-2-yl)-5,

Received: April 25, 2011
Published: June 27, 2011

ACS Publications © 2011 American Chemical Society

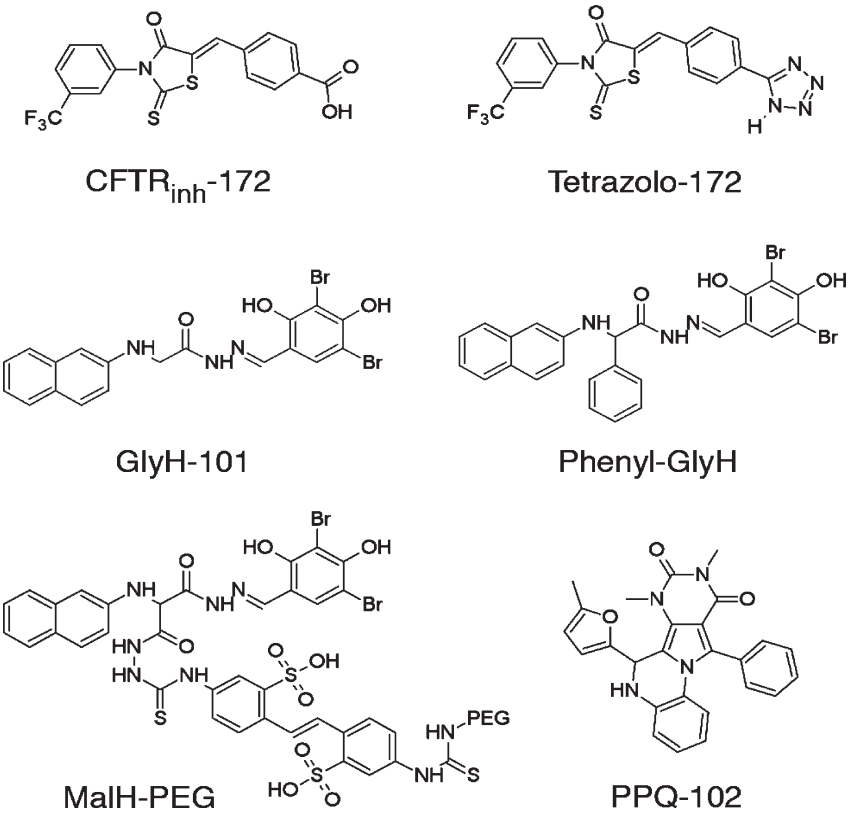

Figure 1. Chemical structures of CFTR inhibitors.

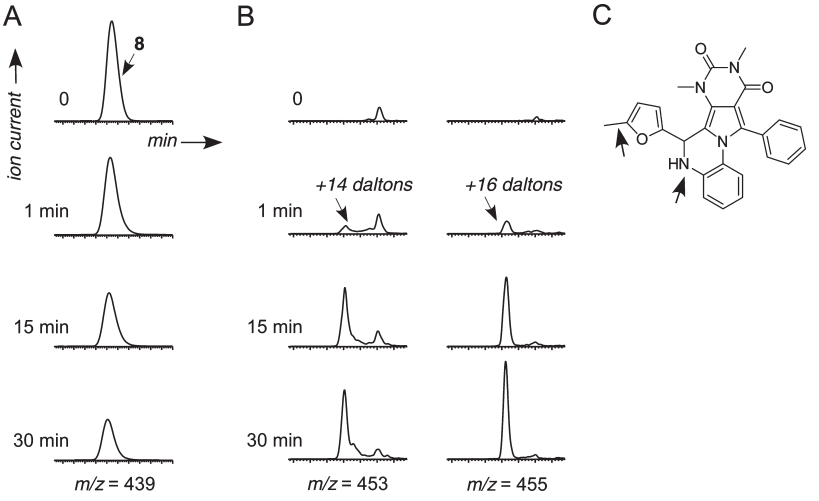

Figure 2. Metabolism of compound **8** in hepatic microsomes. (A) LC/MS showing disappearance over 30 min during incubation with microsomes in the presence of NADPH. (B) Appearance of metabolites at +14 and +16 Da. (C) Schematic of potential sites of metabolism.

6-dihydro-pyrimido-[4′,5′-3,4]pyrrolo[1,2-*a*]quinoxaline-8,10-(7*H*,9*H*)-dione (PPQ-102, Figure 1) **8** inhibited CFTR chloride conductance with IC_{50} ∼ 90 nM by a mechanism involving stabilization of the channel closed-state. PPQ analog **8** prevented cyst expansion and reduced the size of preformed cysts in an embryonic kidney organ culture model of PKD. However, as described below, **8** has poor metabolic stability, precluding animal testing, as well as low polarity (clogP 4.92) and hence low aqueous solubility. To improve compound stability, water solubility, and CFTR inhibition potency, herein we synthesized and characterized a focused library of 27 PPQ and BPO analogues. The most potent compound, **42** (BPO-27) had an IC_{50} ∼ 8 nM for CFTR inhibition, more than 10-fold improved metabolic stability and much greater polarity (clogP 1.76) compared to **8**, and was effective in preventing renal cyst expansion in a PKD model.

RESULTS

We reported **8** as a small-molecule inhibitor of CFTR chloride conductance with efficacy in preventing and reversing cyst

dx.doi.org/10.1021/jm200505e |*J. Med. Chem.* 2011, 54, 5468–5477

Scheme 1. Synthesis of PPQ Analogues[a]

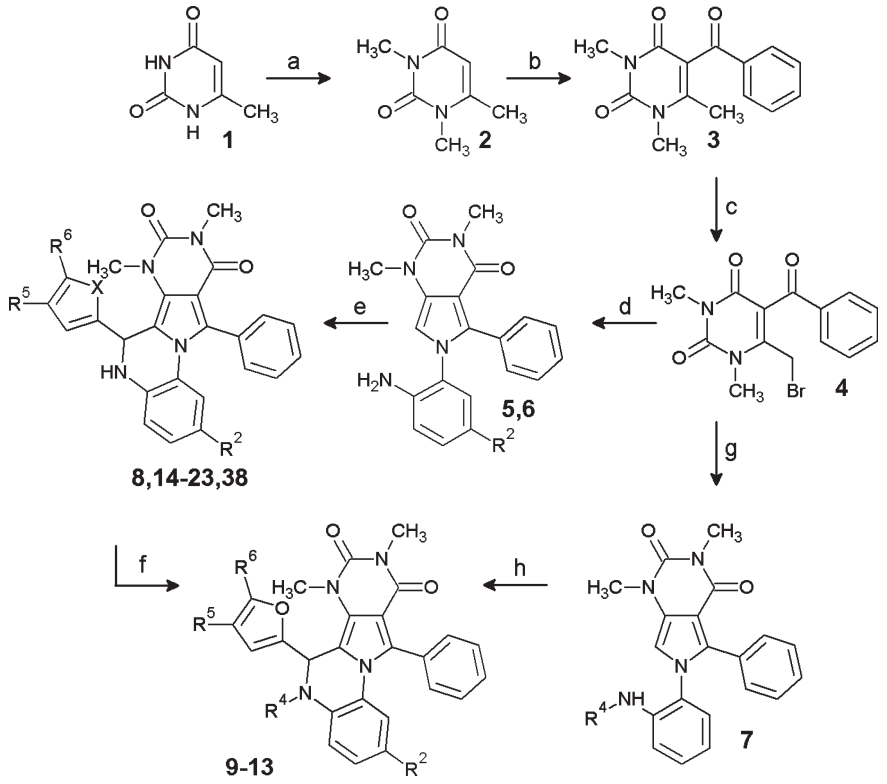

[a] Reagents: (a) NaOH, H_2O, dimethylsulfate, rt, 3 days; (b) benzoyl chloride, $ZnCl_2$, chlorobenzene, reflux; (c) Br_2, CH_2Cl_2, cat. H_2O, reflux; (d) 4-R^2-1,2-phenylenediamine, EtOH, reflux; (e) X═O, R^2 = H, 4-R^5-5-R^6-furfural, 1,2-dichloroethane, TsOH, reflux; X═S, 5-methylthiophene carbaldehyde, 1,2-dichloroethane, TsOH, reflux; X═O, R^2 = NO_2, 5-bromo-2-furaldehyde $CHCl_3$, TFA reflux; (f) R^4 = CH_3SO_2−, methanesulfonyl chloride, DCM, Et_3N; R^4 = $ClCH_2CO$−, chloroacetyl chloride, DCM, Et_3N; R^4 = CH_3CO−, acetic anhydride, DMAP, 100 °C; R^4 = NO, *t*-butyl nitrite, DCM; (g) *N*-methyl-1,2-phenylenediamine, EtOH, reflux; (h) 5-methylfurfural, 1,2-dichloroethane, TsOH, reflux.

formation in an organ culture model of PKD.[30] Preliminary analysis of the metabolic stability and aqueous solubility of **8**, done in preparation for in vivo testing in mouse models of PKD, indicated poor metabolic stability and low water solubility (<2 μM in albumin-free saline). In vitro metabolic stability was determined by compound incubation with hepatic microsomes at 37 °C for specified times in the absence vs presence of NADPH, following by LC/MS analysis. Figure 2A shows loss of **8** in hepatic microsomes in the presence of NADPH, with ~60% disappearance in 30 min. No loss of **8** was seen in the absence of NADPH (data not shown). PPQ analog **8** was undetectable in serum, kidney, and urine at 30−60 min after intravenous bolus administration of 300 μg **8** in mice using an LC/MS assay with sensitivity better than 100 nM (data not shown). Although the precise metabolic fate of **8** is not known, structural considerations and the presence of prominent metabolites at +14 and +16 Da (Figure 2B) suggested possible oxidation, aromatization, and hydroxylation (Figure 2C). To improve on the drug-like properties of **8**, a series analogues was synthesized and tested.

PPQ and BPO Analogue Synthesis. Scheme 1 shows the synthesis of dihydroquinoxoline PPQ (Y═N) compounds and Scheme 2 of benzoxazine BPO (Y═O) compounds. Table 1 shows structures and CFTR inhibition data for all synthesized analogues. Our initial efforts focused on improving the synthesis of **8**, as the original synthesis had low yield.[30] As shown in Scheme 1, 6-methyluracil **1** was exhaustively alkylated using dimethyl sulfate to give 1,3,6-trimethyluracil **2** in 98% yield. 1,3,6-Trimethyluracil **2** was subject to Friedel−Crafts acylation utilizing benzoyl chloride and anhydrous zinc chloride to give ketone **3** in 66% yield. Bromination of ketone **3** gave **4** in quantitative yield. At the first point of diversification, **4** was reacted with substituted 1,2-phenylenediamines (2 equiv) to give pyrroles **5**−**7** in 97% (R^2 = H), 89% (R^2 = NO_2), and 83% (R^4 = Me) yield. Pyrroles **5**−**7** were condensed with the appropriately substituted furfural or thiophene carbaldehyde using catalytic acid to give **13**−**23** and **38** with yields of 57−98%. PPQ analog **8** was obtained on a gram scale in 83% yield. Amide analogues were synthesized from **8** and acid halides or anhydrides to give **9**−**11**, in 73%, 80% and 79% yield, respectively. The nitrosamine **12** was synthesized from **8** and *t*-butyl nitrite in 79% yield.

Scheme 2 shows the synthesis of benzoxazine BPO (Y═O) compounds. Ketone **24** (R^1 = Me) was synthesized from **2** by Friedel−Crafts acylation utilizing *m*-tolyl chloride in 26% yield, and subsequently brominated to give **25** in 93% yield. The condensation of substituted 2-aminophenols with **4** and **25** in ethanol gave pyrroles **26**−**30** in 96% (R^1 = CH_3, R^2 = R^3 = H), 96% (R^1 = R^2 = R^3 = H), 94% (R^1 = R^3 = H, R^2 = NO_2), 88% (R^1 = H, R^2 = Cl, R^3 = NO_2), and 98% (R^1 = R^3 = H, R^2 = COOEt) yield, respectively. Pyrroles **26**−**30** were then condensed with substituted furfurals using catalytic acid at 150 °C to give **31**−**37** and **39**−**41** in yields of 43−84%. BPO analog **40** was

dx.doi.org/10.1021/jm200505e |*J. Med. Chem.* 2011, 54, 5468–5477

Scheme 2. Synthesis of BPO Analogues[a]

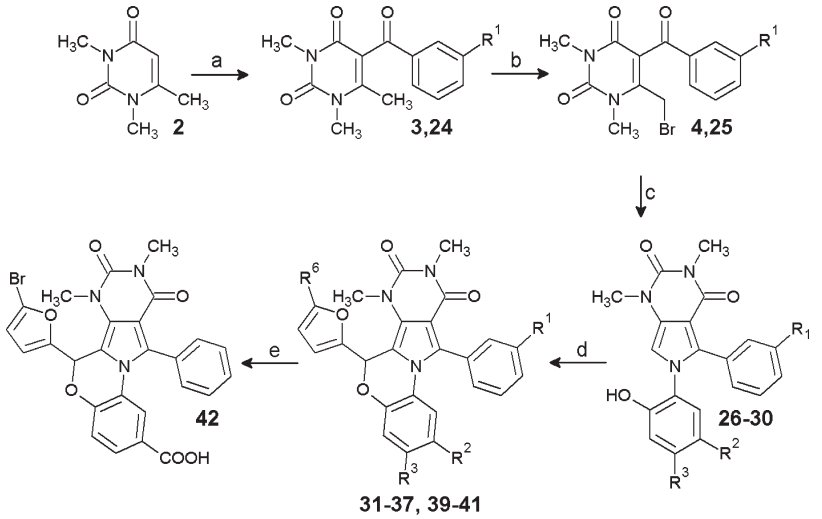

[a] Reagents: (a) R^1 = H, benzoyl chloride, $ZnCl_2$, chlorobenzene, reflux; R^1 = Me, *m*-tolyl chloride, $ZnCl_2$, chlorobenzene, reflux; (b) Br_2, CH_2Cl_2, cat. H_2O, reflux; (c) 2-amino-3-R^2-4-R^3-phenol, EtOH, reflux; (d) 5-R^6-furfual, TFA, $CHCl_3$, or 1,2-dichloroethane, 150 °C; (e) KOH, THF, H_2O, HCl workup.

saponified utilizing KOH in THF and water to give **42** in 83% yield after acid workup.

Characterization of PPQ and BPO Analogues. Initial compound testing for CFTR inhibition was done using a plate-reader assay in which iodide influx was measured in FRT cells coexpressing human wild-type CFTR and the iodide-sensing yellow fluorescent protein YFP-H148Q/I152L. Figure 3A (top) shows representative fluorescence data for inhibition of CFTR-mediated iodide influx by one of the synthesized PPQ analogues, showing reduced negative slope after iodide addition with increasing inhibitor concentration. Figure 3A (bottom) shows concentration−inhibition data for selected compounds, with IC_{50} values for all compounds listed in Table 1. Though relative IC_{50} values are useful for comparisons, absolute IC_{50} values from the plate-reader assay are approximate, generally underestimating compound potency because of assay nonlinearities, pH-dependent YFP fluorescence, the use of iodide instead of chloride, and compound dilution at the start of the assay.[31] Quantitative concentration−inhibition data for the most potent compounds was obtained by analysis of short-circuit current, which represents a definitive electrophysiological measure of compound potency. Current was measured in CFTR-expressing FRT cells in which the basolateral membrane was permeabilized and in the presence of a transepithelial chloride concentration gradient, so that current is a linear measure of CFTR function. CFTR was activated by forskolin, followed by serial additions of increasing concentrations of test compounds. The representative short-circuit current measurement in Figure 3B shows increased CFTR chloride conductance following addition of the cAMP agonist forskolin, which was reduced in a concentration-dependent manner by a PPQ inhibitor, with complete inhibition at high inhibitor concentration.

Our initial synthesis efforts focused on preventing aromatization, which was initially achieved by derivatizing the secondary amine of **8** to give analogues **9**−**13**. The amides **9**−**11** were, however, substantially less active than **8**. As the loss of the basic amine coincided with a loss in activity, we synthesized nitrosamine **12**, but our attempts to reduce the nitrosamine to a strongly basic hydrazine only yielded **8**. To maintain basicity and prevent aromatization, we tried to synthesize the *N*-methyl analogue **13** via reductive alkylation using formaldehyde but were unsuccessful. Fortunately, the *N*-methyl precursor **7** was obtained in good yield from *N*-methyl-1,2-phenylenediamine and **4**. Pyrrole **7** was then used to synthesize **13**, which was weakly active, and so further derivitization at the secondary amine was abandoned.

Re-examination of SAR data obtained from ∼350 commercially available analogues (as reported in ref 30 and unpublished data) suggested that the 5-position of the furan ring in **8** was privileged. Therefore, compounds **14**−**23** were synthesized to probe the steric and electronic requirements for activity of the furyl moiety. Substituting bromine at the 5-position of the furyl ring yielded **18**, which was substantially more stable than **8** and had similar CFTR inhibition potency (Figure 3B,C). To further probe oxidative aromatization as a metabolic pathway, the secondary amine in **18** was replaced by oxygen forming an ether bridge, which is unable to undergo oxidation. The resulting benzoxazine **31** had similar CFTR inhibition potency (Figure 3A) and better stability than **8**. Synthesis of **32**−**33** confirmed the CFTR inhibition activity (Table 1) and improved stability (Figure 3C) imparted by bromine and illustrated the synergy between the 5-bromofuran moiety and the ether bridge.

Previous SAR data[30] showed that an *m*-tolyl moiety (R^1 = Me) increased CFTR inhibition potency. Unfortunately, synthesis of **34**−**35** revealed that the *m*-tolyl moiety reduced CFTR inhibition in the BPO series. To increase the polarity and hence the aqueous solubility of **31**, a nitro group was introduced at R^2. The resulting compound, **36**, had substantially greater CFTR inhibition potency (Figure 4A) with excellent metabolic stability in hepatic microsomes (Figure 4B). BPO analogs **37** and **38** showed that the increased CFTR inhibition activity conferred by the nitro substituent at R^2 was independent of both the 5-bromo substituent and the ether bridge.

To further increase compound polarity, we replaced the nitro functionality at R^2 in **36** with a carboxyl moiety to give **42**. Compound **42** was found the most potent CFTR inhibitor to date with IC_{50} ∼ 8 nM (Figure 4A) and had excellent stability in

dx.doi.org/10.1021/jm200505e |*J. Med. Chem.* 2011, 54, 5468–5477

Table 1. CFTR Inhibition by PPQ and BPO Analogues

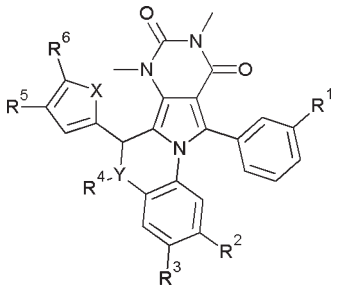

compd	X	Y	R^1	R^2	R^3	R^4	R^5	R^6	IC_{50} (μM)[a]	IC_{50} (μM)[b]
8	O	N	H	H	H	H	H	Me	0.25	0.1
9	O	N	H	H	H	CH_3SO_2	H	Me	inactive	
10	O	N	H	H	H	$ClCH_2CO_2$	H	Me	inactive	
11	O	N	H	H	H	CH_3CO_2	H	Me	inactive	
12	O	N	H	H	H	NO	H	Me	2	
13	O	N	H	H	H	Me	H	Me	1	
14	O	N	H	H	H	H	H	Et	0.3	
15	S	N	H	H	H	H	H	Me	1.7	
16	O	N	H	H	H	H	Me	Me	1.7	
17	O	N	H	H	H	H	H	Cl	0.15	
18	O	N	H	H	H	H	H	Br	0.09	0.05
19	O	N	H	H	H	H	H	I	0.17	0.1
20	O	N	H	H	H	H	H	CF_3	0.35	
21	O	N	H	H	H	H	H	Ph	inactive	
22	O	N	H	H	H	H	H	CH_2OH	inactive	
23	O	N	H	H	H	H	$-(CH)_2-$	$-(CH)_2-$	inactive	
31	O	O	H	H	H		H	Br	0.2	0.09
32	O	O	H	H	H		H	I	0.5	
33	O	O	H	H	H		H	Me	0.15	
34	O	O	Me	H	H		H	Cl	0.37	
35	O	O	Me	H	H		H	Me	0.6	
36	O	O	H	NO_2	H		H	Br	0.12	0.025
37	O	O	H	NO_2	H		H	Me	0.1	0.025
38	O	N	H	NO_2	H	H	H	Br	0.17	
39	O	O	H	Cl	NO_2		H	Me	0.17	
40	O	O	H	COOEt	H		H	Br	0.05	0.025
41	O	O	H	COOEt	H		H	Me	0.08	
42	O	O	H	COOH	H		H	Br	0.04	0.008

[a] By microplate reader assay. [b] By short-circuit current assay.

hepatic microsomes with <5% compound loss in 30 min (Figure 4B). At physiological pH, **42** is deprotonated and thus substantially more polar than **8** (clogP 1.76 vs 4.92), with solubility ~17 μM in a pH 7.4 aqueous phosphate buffer. BPO analog **42** was synthesized by hydrolysis of the ethyl ester **40**, which also strongly inhibited CFTR, and could potentially serve as a pro-drug of **42**.

Inhibition of Cyst Growth in a Kidney Organ Culture Model of PKD. An established embryonic ex vivo kidney organ culture model of PKD was used to test the efficacy of **42** in reducing cAMP agonist-induced renal cystogenesis. Figure 5A shows progressive renal cyst formation and growth in 8-Br-cAMP agonist-treated cultures, as seen by transmitted light microscopy. Kidney growth without cyst formation was seen in the absence of 8-Br-cAMP. Cyst growth in 8-Br-cAMP-treated kidneys was remarkably reduced by inclusion of **42** in the culture medium. As quantified by percentage area occupied by cysts, **42** inhibited cyst growth with IC_{50} ~ 100 nM (Figure 5B), much better than that of >500 nM measured for **8**.[30]

dx.doi.org/10.1021/jm200505e |*J. Med. Chem.* 2011, 54, 5468–5477

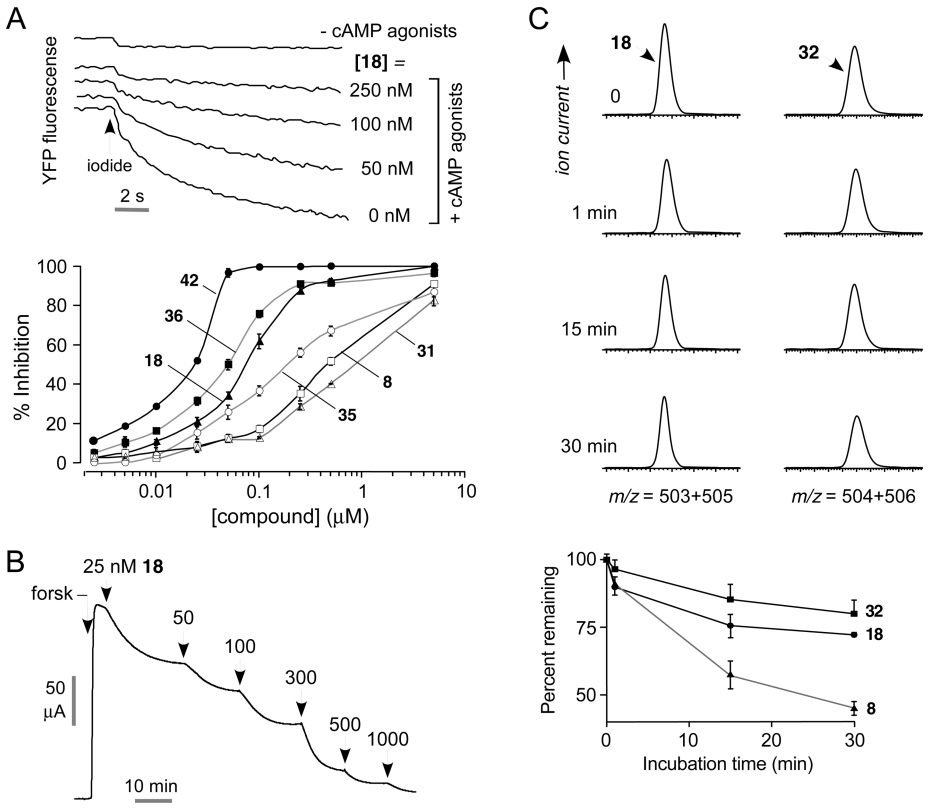

Figure 3. Characterization of PPQ analogues. (A) Fluorescence plate-reader assay of CFTR inhibition. FRT cells expressing human wild-type CFTR and iodide-sensing YFP fluorescent dye were incubated with test compound and CFTR agonists and then subjected to an inwardly directed iodide gradient. (top) Representative data showing kinetics of fluorescence decrease following iodide addition (causing YFP fluorescence quenching) in the absence of cAMP agonists and in the presence of cAMP agonists and indicated concentrations of **18**. (bottom) Summary of concentration−inhibition data for indicated compounds (SE $n = 4$). See Table 1 for IC_{50} values. (B) Short-circuit current analysis of CFTR inhibition in CFTR-expressing FRT cells in the presence of a transepithelial chloride gradient and basolateral membrane permeabilization. Where indicated, forskolin (20 μM) was added to activate CFTR chloride conductance, following by indicated concentrations of **18**. (C) (top) LS/MS analysis showing disappearance of **18** and **32** in hepatic microsomes in the presence of NADPH. (bottom) Summary of kinetics of compound disappearance (SEM, $n = 3$). Data for **8** shown for comparison.

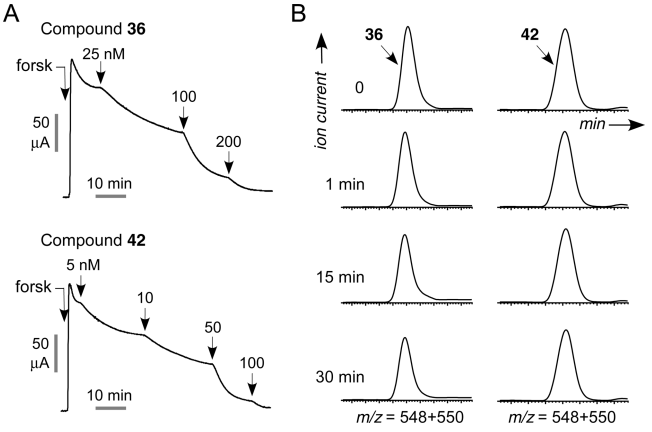

Figure 4. BPO CFTR inhibitors with high potency, metabolic stability, and water solubility. (A) Short-circuit current analysis showing CFTR inhibition by **36** and **42**. (B) Compound stability in hepatic microsomes in the presence of NADPH.

DISCUSSION AND CONCLUSIONS

The best compound emerging from this study, **42**, had substantially improved metabolic stability (by >10-fold) over **8**, as well as greater polarity and potency for inhibition of CFTR chloride conductance in vitro (~10-fold) and renal cystogenesis ex vivo (>5-fold). SAR analysis suggested that the greater stability of **42** over **8** is the consequence of the 5-Br substituted furan and the ether bridge, which largely prevent hydroxylation and aromatization modifications. The greatly improved water solubility of **42** over **8** is a consequence of the carboxylic acid substituent, which is charged at physiological pH. The carboxylic acid addition also, unexpectedly, improved CFTR inhibition potency. The high CFTR inhibition potency of the esterified form of **42**, **40**, suggests its possible use as a pro-drug for efficient intestinal absorption and cell accumulation following de-esterification by ubiquitous intracellular esterases.

Several noteworthy observations were made in synthesizing the PPQ analogues. In an experiment intended to improve yield, bromination of ketone **3** was conducted under strict anhydrous conditions. Ketone **3** was refluxed in CH_2Cl_2 and bromine (1 equiv), but after several hours TLC showed little product. On a whim, several drops of wet CH_2Cl_2 were added to the reaction, which resulted in remarkably rapid discharge of the bromine color and evolution of fuming HBr gas. After several minutes, TLC indicated a near quantitative yield of **4**, which spontaneously crystallized when dried in vacuo. When **4** was condensed

dx.doi.org/10.1021/jm200505e |J. Med. Chem. 2011, 54, 5468–5477

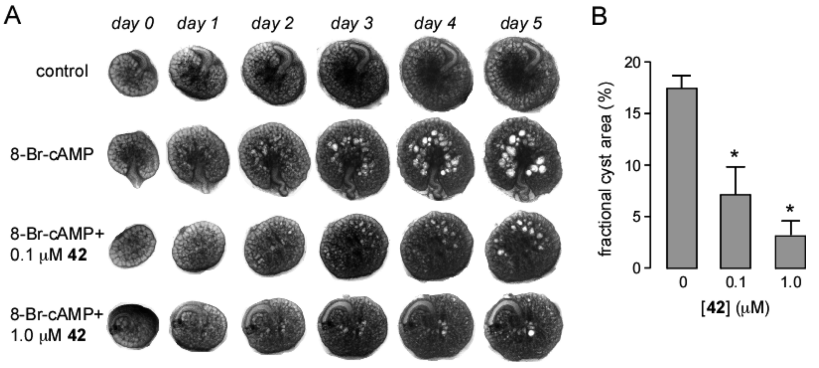

Figure 5. Compound **42** reduces renal cytogenesis. (A) Transmission light micrographs of E13.5 embryonic kidneys cultured for indicated days without or in the presence of 100 μM 8-Br-cAMP, and with 0, 0.1, or 1 μM **42**. (B) Summary of percentage cyst areas at 5 days in cultures (SEM, $n = 4-6$, * $P < 0.001$.

with *N*-methyl-1,2-phenylenediamine, the more reactive secondary amine can undergo alkylation by displacement of the readily accessible bromide in **4**. The high regioselectivity evident in the 83% yield of **5** suggests that the formation of the pyrrole ring in the initial reaction in is one of imine formation rather than alkylation despite the crowded reaction center.

ADPKD is a major health care burden with a prevalence of 1 in 500−1000 individuals.[1] There is no approved drug at present to slow the progression of renal disease in PKD. As mentioned in the Introduction, there is compelling rationale and experimental proof-of-concept for CFTR inhibitor antisecretory therapy for PKD. An alternative antisecretory therapy, vasopressin V2 antagonism, is in clinical trials for PKD and is based on the idea that cysts in PKD often express V2 receptors, which, when stimulated by antidiuretic hormone, elevate cytoplasmic cAMP and activate both CFTR chloride conductance and mTOR signaling.[15,32] Our lab introduced an alternative, V2 receptor-independent strategy to reduce cAMP involving small-molecule phosphodiesterase activators, which were shown to cyst growth in an in vitro PKD model.[33] Pure antiproliferative therapies, most based on the central role of mTOR signaling in proliferation of cyst-lining epithelial cells, are also in clinical trials as well as renin-angiotensin inhibitors and statins.[16−18] Whether antiproliferative or antisecretory therapy alone, or in combination, will slow the progression of kidney destruction in PKD awaits human clinical trials.

Compound **42**, with $IC_{50} \sim 8$ nM, is substantially more potent than existing CFTR inhibitors. In addition to their potential utility for antisecretory therapy of PKD, potent small-molecule CFTR inhibitors have potential efficacy in the therapy of secretory diarrheas and as research tools in defining CFTR-dependent cellular and physiological processes. Secretory diarrheas caused by enterotoxins, such as cholera and travelers' diarrhea (enteropathogenic *E. coli*), require functional CFTR for primary chloride secretion into the intestinal lumen, which secondarily drives sodium and water secretion.[34,35] Testing of **42** and related PPQ analogues is needed to establish their efficacy in animal models of secretory diarrheas, as has been done for thiazolidinone[36] and glycine hydrazide[28,29] CFTR inhibitors. CFTR inhibitors are also useful to create the CF phenotype in ex vivo human and animal tissues, as has been done, for example, in studies of the role of CFTR in airway submucosal gland fluid secretion.[37] Finally, although mouse, pig, and ferret models of CFTR gene deletion exist, pharmacological creation of the CFTR phenotype in animals by CFTR inhibitors might provide complementary data on CFTR function in the absence of compensatory phenomena that can occur in transgenic animal models.

In conclusion, the synthesis and evaluation of a rationally designed series of PPQ analogues produced compounds with much improved metabolic stability, CFTR inhibitory potency, and aqueous solubility compared with reference compound **8**. Compound **42** and related analogues are thus suitable for in vivo testing of efficacy and represent potential development candidates for antisecretory therapy of PKD.

EXPERIMENTAL SECTION

Cell Culture and Platereader Assay of CFTR Inhibition. Fischer rat thyroid (FRT) cells coexpressing human wild-type CFTR and the halide indicator YFP-H148Q were cultured in 96-well black-walled microplates (Corning Costar) at a density of 20000 cells per well in Coon's modified F12 medium containing 10% fetal bovine serum, 2 mM L-glutamine, 100 U/mL penicillin, and 100 μg/mL streptomycin. CFTR chloride conductance was assayed at 48 h after plating on a FluoStar fluorescence plate-reader (BMG Lab Technologies) as described.[21] Each well was washed 3 times with PBS, leaving 60 μL of PBS. Test compounds were added and incubated with the cells for 45 min. Then, 5 μL of a CFTR-activating cocktail (10 μM forskolin, 100 μM IBMX, 20 μM apigenin in PBS) was added. After 15 min, each well was assayed for iodide influx by recording fluorescence continuously (200 ms per point) for 2 s (baseline) and then for 10 s after rapid addition of 160 μL of isosmolar PBS in which 137 mM chloride was replaced by iodide. The initial rate of iodide influx was computed from fluorescence data by nonlinear regression.

Short-Circuit Current. Snapwell inserts containing CFTR-expressing FRT cells were mounted in an Ussing chamber. The hemichambers contained 5 mL of buffer containing 75 mM NaCl and 75 mM Na gluconate (apical) and 150 mM NaCl (basolateral) (pH 7.3), and the basolateral membrane was permeabilized with 250 μg/mL amphotericin B, as described.[27] Short-circuit current was recorded continuously using a DVC-1000 voltage clamp (World Precision Instruments) using Ag/AgCl electrodes and 3 M KCl agar bridges.

Liquid Chromatography/Mass Spectrometry. Compounds (each 5 μM) were incubated for specified times at 37 °C with rat liver microsomes (1 mg protein/mL; Sigma-Aldrich, St. Louis, MO) in potassium phosphate buffer (100 mM) containing NADPH (0 or 1 mM). The mixture was then chilled on ice, and 0.5 mL of ice-cold ethyl acetate was added. Samples were centrifuged for 15 min at 3000 rpm, and the supernatant was evaporated to dryness under nitrogen. The residue was

dissolved in 150 μL mobile phase (acetonitrile:water 3:1, containing 0.1% formic acid) for LC/MS analysis. Reverse-phase HPLC separations were carried out using a Waters C18 column (2.1 mm × 100 mm, 3.5 mm particle size) equipped with a solvent delivery system (Waters model 2690, Milford, MA). The solvent system consisted of a linear gradient from 5 to 95% acetonitrile run over 16 min (0.2 mL/min flow rate). Mass spectra were acquired on an Alliance HT 2790 + ZQ mass spectrometer using negative ion detection, scanning from 150 to 1500 Da. The electrospray ion source parameters were: capillary voltage 3.5 kV (positive ion mode), cone voltage 37 V, source temperature 120 °C, desolvation temperature 250 °C, cone gas flow 25 L/h, and dessolvation gas flow 350 L/h.

Embryonic Organ Culture Model of PKD. Mouse embryos were obtained at embryonic day 13.5 (E13.5). Metanephroi were dissected and placed on transparent Falcon 0.4 mm diameter porous cell culture inserts as described.[30] To the culture inserts was added DMEM/Ham's F-12 nutrient medium supplemented with 2 mM L-glutamine, 10 mM HEPES, 5 μg/mL insulin, 5 μg/mL transferrin, 2.8 nM selenium, 25 ng/mL prostaglandin E, 32 pg/mL T3, 250 U/mL penicillin, and 250 μg/mL streptomycin. Kidneys were maintained in a 37 °C humidified CO_2 incubator for up to 8 days. Culture medium containing 100 μM 8-Br-cAMP, with or without test compound, was replaced (in the lower chamber) every 12 h. Kidneys were photographed using a Nikon inverted microscope (Nikon TE 2000-S) equipped with 2× objective lens, 520 nm bandpass filter, and high-resolution CCD camera. Percentage cyst area was calculated as total cyst area divided by total kidney area.

Synthesis Procedures. NMR spectra (^{1}H at 600 MHz; ^{13}C at 150 MHz) were obtained in methylene chloride (CD_2Cl_2), chloroform ($CDCl_3$), acetonitrile (CD_3CN), or dimethyl sulfoxide (DMSO-d_6) using a 600 MHz Varian spectrometer. Chemical shifts are expressed in parts per million relative to the solvent. NMR spectra for PPQ and BPO compounds were acquired at −20 °C due to excessive broadening of the 11-phenyl protons at ambient temperature. NMR spectra for the intermediates were obtained at ambient temperature. Mass spectrometry was done using a Waters LC/MS instrument with MS, electrospray (+) ionization, mass ranging from 100 to 900 Da, 20 V cone voltage; LC, Xterra MS C_{18} column (2.1 mm × 50 mm × 3.5 μm), 0.2 mL/min water/acetonitrile (containing 0.1% TFA). Purity was judged by the peak area percentage of the UV absorbance signal. Compound purities by RP-HPLC were >98%. Flash chromatography was done using EM silica gel (230−400 mesh), and thin-layer chromatography was done on EMD silica gel 60 F254 plates (Darmstadt, Germany). Melting points are uncorrected. To follow is the synthesis procedure for **42**. See Supporting Information for synthesis of all PPQ and BPO compounds, and analytical data.

*1,3,6-Trimethyl-1H,3H-pyrimidine-2,4-dione (**2**).*[38] In a 250 mL round-bottom flask, 6-methyluracil (**1**; 15.0 g, 119 mmol) and NaOH (9.55 g, 239 mmol) were dissolved in water (150 mL) at low heat. The solution was brought to 25 °C in an ice bath and maintained at 25 °C while dimethyl sulfate (23 mL, 30.59 g, 243 mmol) was added dropwise over 20 min with vigorous stirring. After 22 h, the reaction mixture contained a white precipitate and had pH 9. NaOH (5.0 g, 125 mmol) was added to make the solution homogeneous, and an ice bath was used to maintain a temperature of 25 °C while dimethyl sulfate (12 mL, 15.96 g, 127 mmol) was added dropwise over 10 min. The reaction was stirred for 72 h, then NaOH (2 g, 50 mmol) was added and the reaction extracted with $CHCl_3$ (5 × 50 mL). The chloroform extracts were pooled, dried over Na_2SO_4, and concentrated in vacuo to yield **2** (18 g, 98% yield); mp 114−115 °C. ^{1}H NMR (600 MHz, $CDCl_3$) δ 5.67 (s, 1H), 3.45 (s, 3H), 3.35 (s, 3H), 2.29 (s, 3H). ^{13}C NMR (151 MHz, $CDCl_3$) δ 162.6, 152.5, 151.8, 101.2, 31.9, 28.1, 20.6. MS (ES+) (m/z): $[M + 1]^+$ calculated for $C_7H_{11}N_2O_2$, 155.17, found 155.14.

*5-Benzoyl-1,3,6-trimethylpyrimidine-2,4(1H,3H)-dione (**3**).*[39] In a 100 mL round-bottom flask equipped with a condenser and an air lock was added **2** (5.00 g, 32.4 mmol), anhydrous zinc chloride[40] (freshly dried, 4.45 g, 32.6 mmol), dry chlorobenzene (20 mL), and benzoyl chloride (freshly distilled, 4 mL, 4.84 g, 34.4 mmol). The reaction was refluxed in an oil bath equipped with an air lock and vigorously stirred for 3 h. The reaction was allowed to cool and the condenser arranged for distillation. Water (40 mL) was added dropwise at first and then with increasing speed. Chlorobenzene (30 mL) and water were distilled off, and the mixture was cooled on ice. Diethyl ether (30 mL) was added while stirring, causing a precipitate to form. The precipitate was collected by filtration and recrystallized from 2-propanol (50 mL) to yield **3a** (5.53 g, 66%); mp 143.2−143.7 °C. ^{1}H NMR (600 MHz, CD_3CN) δ 8.74 (d, J = 7.1 Hz, 2H), 8.46 (t, J = 6.0 Hz, 1H), 8.37−8.29 (m, 2H), 4.25 (s, 3H), 4.07 (s, 3H), 2.99 (s, 3H). ^{13}C NMR (151 MHz, CD_3CN) δ 195.6, 162.2, 153.7, 153.2, 139.2, 134.9, 130.5, 130.0, 113.4, 32.8, 28.6, 18.3. MS (ES+) (m/z): $[M + 1]^+$ calculated for $C_{14}H_{15}N_2O_3$, 259.28, found 259.11.

*5-Benzoyl-6-(bromomethyl)-1,3-dimethylpyrimidine-2,4(1H,3H)-dione (**4**).*[39] In a 50 mL round-bottom flask, **3** (1.00 g, 38.7 mmol) was dissolved in CCl_4 (5 mL) and CH_2Cl_2 (4 mL) at 50 °C. Bromine (200 μL, 0.621 g, 38.8 mmol) was mixed with CCl_4 (5 mL) and CH_2Cl_2 (5 mL) in an addition funnel and added dropwise to the solution of **3** such that the brown color disappeared between drops. The last few drops caused the reaction to remain brown. The reaction was then brought to reflux for 10 min before the brown color was discharged by the addition of a few drops of acetone. The reaction was refluxed for 30 min to remove HBr. The reaction was quantitative by TLC, and the product crystallized when concentrated in vacuo to yield **4** (1.305 g, 100%). The product was recrystallized from 2-propanol as colorless needles; mp 171.0−171.7 °C. ^{1}H NMR (600 MHz, CD_2Cl_2) δ 7.88−7.80 (m, 2H), 7.65−7.60 (m, 1H), 7.52−7.45 (m, 2H), 4.24 (s, 2H), 3.59 (s, 3H), 3.31 (s, 3H). ^{13}C NMR (151 MHz, CD_2Cl_2) δ 192.9, 160.9, 152.0, 149.6, 137.8, 134.5, 129.8, 129.2, 114.8, 32.0, 28.6, 23.7. MS (ES+) (m/z): $[M + 1]^+$ calculated for $C_{14}H_{14}BrN_2O_3$, 338.18, found 338.81.

*Ethyl 3-(1,3-Dimethyl-2,4-dioxo-5-phenyl-3,4-dihydro-1H-pyrrolo-[3,4-d]pyrimidin-6(2H)-yl)-4-hydroxybenzoate (**30**).* In a 100 mL round-bottom flask, ethyl 3-amino-4-hydroxybezoate (1.10 g, 6.07 mmol) and **4** (1.00 g, 2.98 mmol) were refluxed in ethanol (50 mL). After 2 h, the condenser was rearranged for distillation, and ethanol (25 mL) was distilled off. The resulting solution was slowly poured into a vigorously stirred solution of ice-cold water (200 mL) and citric acid (50 mg), giving a pink solid precipitate. The mixture was stirred for 10 min, and then the solid was collected by filtration and rinsed with cold water to give **30** (1.23 g, 98.5%) after drying; mp 129.2−130 °C. ^{1}H NMR (600 MHz, CD_2Cl_2) δ 8.58 (s, 1H), 7.89 (dd, J = 2.1 Hz, 8.7, 1H), 7.67 (d, J = 2.1 Hz, 1H), 7.36−7.29 (m, 2H), 7.28−7.18 (m, 3H), 6.97 (d, J = 8.7 Hz, 1H), 4.25 (q, J = 7.1 Hz, 2H), 3.27 (s, 3H), 3.17 (s, 3H), 1.30 (t, J = 7.1 Hz, 3H). ^{13}C NMR (151 MHz, CD_2Cl_2) δ 165.4, 159.7, 156.8, 151.9, 136.1, 132.1, 130.9, 130.7, 129.5, 129.0, 128.8, 127.8, 125.7, 122.9, 117.7, 104.7, 103.1, 61.2, 32.0, 28.1, 14.2. MS (ES+) (m/z): $[M + 1]^+$ calculated for $C_{23}H_{22}N_3O_5$, 420.16, found 420.13.

*Ethyl 6-(5-Bromofuran-2-yl)-7,9-dimethyl-8,10-dioxo-11-phenyl-7,8,9,10-tetrahydro-6H-benzo[b]pyrimido [4′,5′:3,4]pyrrolo[1,2-d]-[1,4]oxazine-2-carboxylate (**40**).* Pyrrole **30** (500 mg, 1.19 mmol), 5-bromofurfural (240 mg, 1.37 mmol), chloroform (7 mL), TFA (10 μL, 14.8 mg, 130 μmol), and 3 Å molecular sieves (2.0 g, 8−12 mesh beads) were sealed in an Emrys 10−20 mL process vial and submerged to the level of solvent in an oil bath at 150 °C. The reaction was stirred for 24 min and then removed from the oil bath. Once the internal pressure dropped the reaction vial was rapidly cooled in water. After cooling, the reaction was filtered through Celite into a 50 mL recovery flask and then dried in vacuo. The residue was dissolved in a minimum amount of CH_2Cl_2 and quickly diluted with warm ethanol (25 mL). Fine crystals began to form immediately. The mixture was then placed on a rotary

evaporator, and the CH_2Cl_2 was removed to increase the quantity of crystals. The mixture was then chilled, filtered, and the crystals rinsed with cold ethanol to give **40** (0.500 g, 76.4%) as fine white needle-like crystals. No mp (slow decomposition). ^{1}H NMR (600 MHz, CD_2Cl_2) δ 7.81 (d, J = 7.7 Hz, 1H), 7.68 (dd, J = 1.9 Hz, 8.4, 1H), 7.63 (t, J = 7.5 Hz, 1H), 7.52 (t, J = 7.5 Hz, 1H), 7.34 (t, J = 7.5 Hz, 1H), 7.23 (d, J = 1.8 Hz, 1H), 7.09 (d, J = 8.4 Hz, 1H), 7.06 (d, J = 7.7 Hz, 1H), 6.86 (s, 1H), 6.14 (d, J = 3.4 Hz, 1H), 5.98 (d, J = 2.9 Hz, 1H), 4.11 (dq, J = 7.2 Hz, 10.7, 1H), 4.00 (dq, J = 7.1 Hz, 10.7, 1H), 3.48 (s, 3H), 3.26 (s, 3H), 1.14 (t, J = 7.1 Hz, 3H). ^{13}C NMR (151 MHz, CD_2Cl_2) δ 165.0, 159.3, 151.9, 151.8, 149.1, 131.8, 131.3, 130.0, 129.8, 129.7, 128.8, 128.8, 128.3, 125.4, 124.7, 124.5, 124.4, 121.6, 119.6, 114.9, 112.4, 105.9, 105.7, 68.4, 61.3, 32.4, 28.0, 14.2. MS (ES+) (m/z): $[M + 1]^+$ calculated for $C_{28}H_{23}BrN_3O_6$, 576.08, found 576.04.

*6-(5-Bromofuran-2-yl)-7,9-dimethyl-8,10-dioxo-11-phenyl-7,8,9,10-tetrahydro-6H-benzo[b]pyrimido [4′,5′:3,4]pyrrolo[1,2-d][1,4]oxazine-2-carboxylic Acid (**42**).* In a 500 mL round-bottom flask equipped with stir bar, **40** (1.00 g, 1.73 mmol) was dissolved in THF (100 mL) with gentle heat and then allowed to cool. A mixture of water (70 mL) and KOH (768 mg, 13.7 mmol) was quickly added to the vigorously stirred solution, which formed a white suspension. After 3 days, the mixture was a homogeneous yellow solution free of **40** as determined by LC/MS. The THF was removed using a rotary evaporator and warm water bath, leaving behind a viscous aqueous solution. The solution was made strongly acidic to litmus using 1% aq HCl while stirring vigorously with a glass rod. The resulting gel was shaken with EtOAc (125 mL) and then quickly poured into a 1 L separatory funnel, where a precipitate formed in the organic layer. The 500 mL flask was rinsed with additional EtOAc (125 mL). Additional EtOAc (400 mL) was added until all solids dissolved. After settling, the lower yellow aqueous layer was discarded. The EtOAc layer was washed with brine, dried over Na_2SO_4, and dried on a rotary evaporator. The resulting slightly yellow amorphous powder was loosened by swirling with CH_2Cl_2 (15 mL) and then diluted with diethyl ether (15 mL). The solids were collected by filtration and rinsed with CH_2Cl_2:Et_2O (1:1) to give **42** (791 mg, 83.2%) as a white solid. No mp (slow decomposition). ^{1}H NMR (600 MHz, 91% CD_2Cl_2, 9% DMSO-d_6) δ 12.30 (s, 1H), 7.79 (d, J = 7.7 Hz, 1H), 7.63 (dd, J = 1.9 Hz, 8.4, 1H), 7.58 (t, J = 7.6 Hz, 1H), 7.46 (t, J = 7.5 Hz, 1H), 7.29 (t, J = 7.5 Hz, 1H), 7.17 (d, J = 1.7 Hz, 1H), 7.04 (d, J = 8.4 Hz, 1H), 7.01 (d, J = 7.7 Hz, 1H), 6.89 (s, 1H), 6.12 (d, J = 3.4 Hz, 1H), 5.96 (d, J = 3.3 Hz, 1H), 3.44 (s, 3H), 3.21 (s, 3H). ^{13}C NMR (151 MHz, 91% CD_2Cl_2, 9% DMSO-d_6) δ 166.7, 159.1, 151.9, 151.6, 149.0, 131.8, 131.0, 129.7, 129.7, 129.5, 128.6, 128.5, 128.5, 125.3, 125.2, 124.4, 124.2, 121.9, 119.4, 114.8, 112.3, 106.0, 105.7, 68.2, 32.3, 27.8. MS (ES+) (m/z): $[M + 1]^+$ calculated for $C_{26}H_{19}BrN_3O_6$, 548.05, found 548.00.

■ ASSOCIATED CONTENT

Supporting Information. Detailed synthesis procedures and NMR spectra for all compounds. This material is available free of charge via the Internet at http://pubs.acs.org.

■ AUTHOR INFORMATION

Corresponding Author

*Phone: 415-4768530. Fax: 415-6653847. E-mail: alan.verkman@ucsf.edu. Webstie: http://www.ucsf.edu/verklab. Address: University of California, San Francisco, Box 0521, HSE 1246, 513 Parnassus Avenue, San Francisco, CA 94143-0521.

■ ACKNOWLEDGMENT

This work was supported by NIH grants DK86125, DK72517, HL73856, EB00415, DK35124, and EY13574 and Research Development Program and Drug Discovery grants from the Cystic Fibrosis Foundation.

■ ABBREVIATIONS USED

ADPKD, autosomal dominant polycystic kidney disease; BPO, benzopyrimido-pyrrolo-oxazinedione; CFTR, cystic fibrosis transmembrane conductance regulator; CPT-cAMP, chlorophenylthio-cAMP; IBMX, isobutylmethylxanthine; PKD, polycystic kidney disease; PPQ, pyrimido-pyrrolo-quinoxalinedione; YFP, yellow fluorescent protein

■ REFERENCES

(1) Torres, V. E.; Harris, P. C.; Pirson, Y. Autosomal dominant polycystic kidney disease. *Lancet* **2007**, *369*, 1287–1301.

(2) Grantham, J. J.; Chapman, A. B.; Torres, V. E. Volume progression in autosomal dominant polycystic kidney disease: the major factor determining clinical outcomes. *Clin. J. Am. Soc. Nephrol.* **2006**, *1*, 148–157.

(3) Ye, M.; Grantham, J. J. The secretion of fluid by renal cysts from patients with autosomal dominant polycystic kidney disease. *N. Engl. J. Med.* **1993**, *329*, 310–313.

(4) Hanaoka, K.; Guggino, W. B. cAMP regulates cell proliferation and cyst formation in autosomal polycystic kidney disease cells. *J. Am. Soc. Nephrol.* **2000**, *11*, 1179–1187.

(5) Magenheimer, B. S.; St John, P. L.; Isom, K. S.; Abrahamson, D. R.; De Lisle, R. C.; Wallace, D. P.; Maser, R. L.; Grantham, J. J.; Calvet, J. P. Early embryonic renal tubules of wild-type and polycystic kidney disease kidneys respond to cAMP stimulation with cystic fibrosis transmembrane conductance regulator/$Na^+K^+2Cl^-$ cotransporter-dependent cystic dilation. *J. Am. Soc. Nephrol.* **2006**, *17*, 3424–3437.

(6) Riordan, J. R. CFTR function and prospects for therapy. *Annu. Rev. Biochem.* **2008**, *77*, 701–726.

(7) Brill, S. R.; Ross, K. E.; Davidow, C. J.; Ye, M.; Grantham, J. J.; Caplan, M. J. Immunolocalization of ion transport proteins in human autosomal dominant polycystic kidney epithelial cells. *Proc. Natl. Acad. Sci. U.S.A.* **1996**, *93*, 10206–10211.

(8) Davidow, C. J.; Maser, R. L.; Rome, L. A.; Calvet, J. P.; Grantham, J. J. The cystic fibrosis transmembrane conductance regulator mediates transepithelial fluid secretion by human autosomal dominant polycystic kidney disease epithelium in vitro. *Kidney Int.* **1996**, *50*, 208–218.

(9) Li, H.; Findlay, I. A.; Sheppard, D. N. The relationship between cell proliferation, Cl-secretion, and renal cyst growth: a study using CFTR inhibitors. *Kidney Int.* **2004**, *66*, 1926–1938.

(10) Cotton, C. U.; Avner, E. D. PKD and CF: an interesting family provides insight into the molecular pathophysiology of polycystic kidney disease. *Am. J. Kidney Dis.* **1998**, *32*, 1081–1083.

(11) O'Sullivan, D. A.; Torres, V. E.; Gabow, P. A.; Thibodeau, S. N.; King, B. F.; Bergstralh, E. J. Cystic fibrosis and the phenotypic expression of autosomal dominant polycystic kidney disease. *Am. J. Kidney Dis.* **1998**, *32*, 976–983.

(12) Xu, N.; Glockner, J. F.; Rossetti, S.; Babovich-Vuksanovic, D.; Harris, P. C.; Torres, V. E. Autosomal dominant polycystic kidney disease coexisting with cystic fibrosis. *J. Nephrol.* **2006**, *19*, 529–534.

(13) Lieberthal, W.; Levine, J. S. The role of the mammalian target of rapamycin (mTOR) in renal disease. *J. Am. Soc. Nephrol.* **2009**, *20*, 2493–2502.

(14) Torres, V. E.; Boletta, A.; Chapman, A.; Gattone, V.; Pei, Y.; Qian, Q.; Wallace, D. P.; Weimbs, T.; Wuthrich, R. P. Prospects for mTOR inhibitor use in patients with polycystic kidney disease and hamartomatous diseases. *Clin. J. Am. Soc. Nephrol.* **2010**, *5*, 1312–1329.

(15) Belibi, F. A.; Edelstein, C. L. Novel targets for the treatment of autosomal dominant polycystic kidney disease. *Expert Opin. Invest. Drugs.* **2010**, *19*, 315–328.

(16) Masoumi, A.; Reed-Gitomer, B.; Kelleher, C.; Schrier, R. W. Potential pharmacological interventions in polycystic kidney disease. *Drugs* **2007**, *67*, 2495–2510.

(17) Patel, V.; Chowdhury, R.; Igarashi, P. Advances in the pathogenesis and treatment of polycystic kidney disease. *Curr. Opin. Nephrol. Hypertens.* **2009**, *18*, 99–106.

(18) Torres, V. E. Treatment strategies and clinical trial design in ADPKD. *Adv. Chronic Kidney Dis.* **2010**, *17*, 190–204.

(19) Verkman, A. S.; Galietta, L. J. Chloride channels as drug targets. *Nature Rev. Drug Discovery* **2009**, *8*, 153–171.

(20) Caci, E.; Caputo, A.; Hinzpeter, A.; Arous, N.; Fanen, P.; Sonawane, N.; Verkman, A. S.; Ravazzolo, R.; Zegarra-Moran, O.; Galietta, L. J. Evidence for direct CFTR inhibition by CFTR(inh)-172 based on Arg347 mutagenesis. *Biochem. J.* **2008**, *413*, 135–142.

(21) Ma, T.; Thiagarajah, J. R.; Yang, H.; Sonawane, N. D.; Folli, C.; Galietta, L. J.; Verkman, A. S. Thiazolidinone CFTR inhibitor identified by high-throughput screening blocks cholera toxin-induced intestinal fluid secretion. *J. Clin. Invest.* **2002**, *110*, 1651–1658.

(22) Taddei, A.; Folli, C.; Zegarra-Moran, O.; Fanen, P.; Verkman, A. S.; Galietta, L. J. Altered channel gating mechanism for CFTR inhibition by a high-affinity thiazolidinone blocker. *FEBS Lett.* **2004**, *558*, 52–56.

(23) Sonawane, N. D.; Muanprasat, C.; Nagatani, R., Jr.; Song, Y.; Verkman, A. S. In vivo pharmacology and antidiarrheal efficacy of a thiazolidinone CFTR inhibitor in rodents. *J. Pharm. Sci.* **2005**, *94*, 134–143.

(24) Sonawane, N. D.; Verkman, A. S. Thiazolidinone CFTR inhibitors with improved water solubility identified by structure–activity analysis. *Bioorg. Med. Chem.* **2008**, *16*, 8187–8195.

(25) Yang, B.; Sonawane, N. D.; Zhao, D.; Somlo, S.; Verkman, A. S. Small-molecule CFTR inhibitors slow cyst growth in polycystic kidney disease. *J. Am. Soc. Nephrol.* **2008**, *19*, 1300–1310.

(26) Muanprasat, C.; Sonawane, N. D.; Salinas, D.; Taddei, A.; Galietta, L. J.; Verkman, A. S. Discovery of glycine hydrazide pore-occluding CFTR inhibitors: mechanism, structure–activity analysis, and in vivo efficacy. *J. Gen. Physiol.* **2004**, *124*, 125–137.

(27) Sonawane, N. D.; Hu, J.; Muanprasat, C.; Verkman, A. S. Luminally active, nonabsorbable CFTR inhibitors as potential therapy to reduce intestinal fluid loss in cholera. *FASEB J.* **2006**, *20*, 130–132.

(28) Sonawane, N. D.; Zhao, D.; Zegarra-Moran, O.; Galietta, L. J.; Verkman, A. S. Nanomolar CFTR inhibition by pore-occluding divalent polyethylene glycol-malonic acid hydrazides. *Chem. Biol.* **2008**, *15*, 718–728.

(29) Sonawane, N. D.; Zhao, D.; Zegarra-Moran, O.; Galietta, L. J.; Verkman, A. S. Lectin conjugates as potent, nonabsorbable CFTR inhibitors for reducing intestinal fluid secretion in cholera. *Gastroenterology.* **2007**, *132*, 1234–1244.

(30) Tradtrantip, L.; Sonawane, N. D.; Namkung, W.; Verkman, A. S. Nanomolar potency pyrimido-pyrrolo-quinoxalinedione CFTR inhibitor reduces cyst size in a polycystic kidney disease model. *J. Med. Chem.* **2009**, *52*, 6447–6455.

(31) Galietta, L. V.; Jayaraman, S.; Verkman, A. S. Cell-based assay for high-throughput quantitative screening of CFTR chloride transport agonists. *Am. J. Physiol.: Cell Physiol.* **2001**, *281*, C1734–C1742.

(32) Torres, V. E. Role of vasopressin antagonists. *Clin. J. Am. Soc. Nephrol.* **2008**, *3*, 1212–1218.

(33) Tradtrantip, L.; Yangthara, B.; Padmawar, P.; Morrison, C.; Verkman, A. S. Thiophenecarboxylate suppressor of cyclic nucleotides discovered in a small-molecule screen blocks toxin-induced intestinal fluid secretion. *Mol. Pharmacol.* **2009**, *75*, 134–142.

(34) Kunzelmann, K.; Mall, M. Electrolyte transport in the mammalian colon: mechanisms and implications for disease. *Physiol. Rev.* **2002**, *82*, 245–289.

(35) Thiagarajah, J. R.; Verkman, A. S. CFTR pharmacology and its role in intestinal fluid secretion. *Curr. Opin. Pharmacol.* **2003**, *3*, 594–599.

(36) Thiagarajah, J. R.; Broadbent, T.; Hsieh, E.; Verkman, A. S. Prevention of toxin-induced intestinal ion and fluid secretion by a small-molecule CFTR inhibitor. *Gastroenterology.* **2004**, *126*, 511–519.

(37) Thiagarajah, J. R.; Song, Y.; Haggie, P. M.; Verkman, A. S. A small molecule CFTR inhibitor produces cystic fibrosis-like submucosal gland fluid secretions in normal airways. *FASEB J.* **2004**, *18*, 875–877.

(38) Azas, N.; Rathelot, P.; Djekou, S.; Delmas, F.; Gellis, A.; Di Giorgio, C.; Vanelle, P.; Timon-David, P. Antiparasitic activity of highly conjugated pyrimidine-2,4-dione derivatives. *Farmaco* **2003**, *58*, 1263–1270.

(39) Tsupak, E. B. Pyrrolopyrimidines. 5. Reaction of 6-amino-1,3-dimethylpyrrolo[3,4-*d*]pyrimidine-2,4(1*H*,3*H*)-diones with 1,3-diketones. *Chem. Heterocycl. Compd.* **2003**, *39*, 953–959.

(40) Pray, A. P. In *Inorganic Syntheses*; J. Wiley & Sons: New York, 1990; Vol. XXVIII, pp 321−322.